ORIGINAL RESEARCH

MR Imaging of Orbital Inflammatory Syndrome, Orbital Cellulitis, and Orbital Lymphoid Lesions: The Role of Diffusion-Weighted Imaging

R. Kapur
A.R. Sepahdari
M.F. Mafee
A.M. Putterman
V. Aakalu
L.J.A. Wendel
P. Setabutr

BACKGROUND AND PURPOSE: Orbital inflammatory syndrome (OIS) has clinical features that overlap with orbital lymphoid lesions and orbital cellulitis. Prompt diagnosis is needed in all 3 conditions because the management of each one differs greatly. CT and MR imaging, though useful, do not always distinguish among these conditions. The aim of this study was to identify the role of diffusion-weighted imaging (DWI) in differentiating these 3 diagnoses.

MATERIALS AND METHODS: A retrospective analysis of orbital MR imaging was conducted. T1- and T2-weighted and postcontrast images were analyzed. Region-of-interest analysis was performed by using measurements in areas of abnormality seen on conventional MR imaging sequences and measurements of the ipsilateral thalamus for each patient. The DWI signal intensity of the lesion was expressed as a percentage of average thalamic intensity in each patient. Similarly, lesion apparent diffusion coefficients (ADCs) and lesion-thalamus ADC ratios were calculated. Statistical significance was determined by the Kruskal-Wallis test, and post hoc pairwise comparisons, by the Mann-Whitney *U* test for DWI-intensity ratio, ADC, and ADC ratio.

RESULTS: A significant difference was noted in DWI intensities, ADC, and ADC ratio between OIS, orbital lymphoid lesions, and orbital cellulitis ($P < .05$). Lymphoid lesions were significantly brighter than OIS, and OIS lesions were significantly brighter than cellulitis. Lymphoid lesions showed lower ADC than OIS and cellulitis. A trend was seen toward lower ADC in OIS than in cellulitis ($P = .17$).

CONCLUSIONS: DWI may help differentiate OIS from lymphoid lesions and cellulitis and may allow more rapid management.

Orbital inflammatory syndrome (OIS), commonly known as inflammatory orbital pseudotumor, is the most common cause of non-thyroid-related noninfectious orbital disease.[1] Other processes, specifically orbital lymphoid lesions and orbital cellulitis, can frequently masquerade as OIS.[2-5]

Orbital lymphoid lesions generally present with a progressive course of low-grade proptosis and minimal pain. OIS generally presents more acutely, with symptoms of proptosis, extraocular motility disturbance, pain, erythema, and chemosis.[2] Nonetheless, all of these features can be common to both OIS and orbital lymphoid lesions with a variable onset seen in both processes. Orbital lymphoid lesion commonly presents as a mass on CT and MR imaging. However, an inflammatory presentation of lymphoma is often seen.[5] Furthermore, OIS can also appear as a mass, further complicating the distinction between these diseases.[4]

Orbital cellulitis also can present with clinical findings similar to those of OIS, and differentiating the 2 may be challenging. Orbital cellulitis is frequently associated with a history of sinusitis, trauma, recent dental work, orbital fracture, scleral buckling, or strabismus surgery. Pain and fever are variably present. On imaging, both can appear as a diffuse inflammatory process, further adding to the confusion.[3]

Prompt diagnosis is needed in all 3 conditions, and the management differs greatly, stressing the importance of early diagnosis. CT imaging of OIS shows unpredictable attenuation and varying degrees of contrast enhancement.[4] Although T1- and T2-weighted MR imaging sequences can be useful, the signal intensities in these sequences can overlap, and these lesions are not always readily differentiated. Previous descriptive analyses comparing OIS and lymphoma, and comparing OIS and orbital cellulitis on MR imaging, did not show differences specific enough for differentiating these diseases.[2,6]

Because the clinical findings and conventional MR imaging findings in OIS, orbital lymphoid lesions, and orbital cellulitis often have considerable overlap, it can be difficult to make a definitive diagnosis without a pathologic specimen. Therefore, it would be clinically useful to have a noninvasive method to help distinguish these processes.

Diffusion-weighted imaging (DWI) is an MR imaging technique that was described as early as 1986 and is most commonly used to identify acutely infarcted cerebral tissue, which has an increased intracellular fraction of water.[7] In recent years, additional investigation has focused on the utility of DWI in characterizing a number of lesions including lymphoma, abscesses, and glioblastoma multiforme, including

Received May 7, 2008; accepted after revision August 10.

From the Departments of Ophthalmology and Visual Sciences (R.K., A.M.P., V.A., P.S.) and Radiology (A.R.S.), University of Illinois at Chicago, Chicago, Ill; Department of Radiology (M.F.M.), University of California, San Diego, Calif; and Department of Ophthalmology and Visual Sciences (L.J.A.W.), University of Iowa, Iowa City, Iowa.

Drs Kapur and Sepahdari shared an equal role in the design and authorship of this study.

The work was supported in part by Opthalmology Departmental Core Grant P30 EY001792, National Institutes of Health, Bethesda, Md.

Paper previously presented at: Fall Scientific Symposium of the American Society of Ophthalmic Plastic and Reconstructive Surgery, November 9–10, 2007, New Orleans, La.; Pinsky Resident Research competition, March 15, 2008, Chicago, Ill; American Society of Head and Neck Radiology, September 26–30, 2007, Seattle, Wash.

Please address correspondence to Rashmi Kapur, MD, Department of Ophthalmology and Visual Sciences, University of Illinois at Chicago, 1855 W Taylor St, M/C 648, Chicago, IL 60612; e-mail: rashmi_kapur@yahoo.com

DOI 10.3174/ajnr.A1315

correlation with histopathology.[8-13] It is likely that the mechanisms governing diffusion restriction are more complex than the simple intracellular fraction of water and may additionally relate to the presence of proteins and extracellular molecules that increase tissue viscosity.[14]

We chose to investigate the application of DWI in the diagnosis of OIS, orbital lymphoid lesions, and orbital cellulitis. Because reactive lymphoid lesions overlap with malignant lymphoma by histology and imaging, they were compiled into 1 group called "orbital lymphoid lesions."[15] Our hypotheses are that lymphoid lesions will restrict diffusion more than OIS due to an increased intracellular fraction of water and that orbital cellulitis will restrict diffusion less than OIS because we believe that the radiographic abnormality in cellulitis reflects edema related to increased capillary permeability rather than a cellular infiltrate. We also studied and compared conventional T1 and T2 signal-intensity differences among these lesions to see if a clear distinction was possible without DWI.

Materials and Methods

With institutional review board approval and a waiver of informed consent, a retrospective analysis of orbital MR imaging performed over a 7-year period was conducted. Two search methods were used to identify subjects with a diagnosis of orbital cellulitis, OIS, and orbital lymphoid lesions. Using PACS, the keywords "cellulitis," "pseudotumor," and "lymphoma" were searched in "Study Indications" and "Findings." Patients with MR imaging and DWI series were selected. The clinic records of the oculoplastics department were similarly searched for relevant terms. These included malignant neoplasm of the orbit (190.1), benign neoplasm of the orbit (224.1), benign neoplasm of lacrimal gland (224.2), neoplasm not otherwise specified (239.8), uncertain behavior neoplasm (238.8), orbital granuloma/pseudotumor (376.11), exophthalmos unspecified (376.30), and orbital cellulitis (376.01). After this initial identification of 405 patients, patients' electronic medical records were reviewed to determine if they had undergone MR imaging. Inclusion criteria consisted of a diagnosis of 1 of the previously mentioned conditions by surgical pathology, when available, or clinical evidence based on treatment and course; and orbital MR imaging, including whole-brain DWI. Clinical criteria for OIS included a response to corticosteroids as well as an unrevealing search for other causes of orbital inflammatory process with at least 3 months of follow-up. Clinical criteria for cellulitis included culture of a suggested pathogen and/or a sustained response to antimicrobial therapy. Patients were then grouped by diagnosis, representing the initial analysis group of 20 patients (7 OIS, 8 cellulitis, 5 orbital lymphoid lesions).

In addition to axial whole-brain DWI, our standard orbit protocol included the following conventional whole-brain sequences: axial fast spin-echo T2, T2 fluid-attenuated inversion recovery, and spin-echo T1 postcontrast. Conventional high-resolution orbit sequences included axial fast spin-echo T2, T1 without contrast, T1 postcontrast, T1 fat-suppressed postcontrast, coronal fat-suppressed T1 postcontrast, and oblique parasagittal T1 fat-suppressed postcontrast.

The conventional sequences were reviewed to assess the location and appearance of the lesion. For patients with orbital cellulitis, areas of nonspecific inflammation were analyzed and areas with abscesses were excluded. If a lesion (OIS, orbital cellulitis, or lymphoid lesion) was visible within the resolution of the conventional whole-brain images, the DWI sequences were then analyzed. Two patients were excluded because of abnormalities that were not detectable within the resolution of the whole-brain sequences (1 OIS, 1 lymphoma). One patient was excluded because the lesion was not included in the DWI sequence (1 OIS). One patient was excluded because of susceptibility artifact that overlay degraded DWI image quality (1 OIS). Two patients with cellulitis were excluded because of imaging findings that showed no overlap with either OIS or lymphoma (large frank abscess in both cases, without a distinct region of nonspecific inflammation). The final study group consisted of 14 patients (4 OIS, 6 cellulitis, 4 lymphoma), 10 females and 4 males. The group had a median age at presentation of 48 years (range, 9–70 years).

Twelve patients were imaged on a Signa 1.5T magnet, and 2 were imaged on a Signa 3T magnet (GE Healthcare, Milwaukee, Wis) by using an 8-channel head coil. A single-shot spin-echo echo-planar DWI sequence was performed with b-values of 0 and 1000 s/mm^2, 128 × 128 matrix, 28-cm FOV, 5-mm section thickness, and 5-mm section spacing. Parallel acquisition was performed in 13 of 14 patients by using array spatial sensitivity encoding technique (ASSET). Routine software correction for eddy current distortion was applied. Automated apparent diffusion coefficient (ADC) maps and exponential ADC maps without quantitative ADC were created in 11 of 14 patients on the GE workstation. ADC maps were not created in 3 patients per existing MR imaging protocol at that time.

DWI sequences were cross-referenced with conventional sequences in multiple planes for lesion localization, and region-of-interest analysis was performed by using manual oval region-of-interest measurements (~10 mm^2) in the areas of abnormality. Four intensity measurements were obtained for each lesion on $b = 1000$ sequences (I) and on $b = 0$ sequences (I0). Four similar-sized regions of interest were also obtained from the ipsilateral thalamus of each patient in a similar fashion. The average lesion DWI intensity was expressed as a percentage of average thalamic intensity in each patient, producing a DWI ratio similar to that in a previously described technique.[16] Quantitative ADC was determined by manual calculation by using region-of-interest intensity on $b = 1000$ and $b = 0$ sequences according to the equation: ADC = ln (I0 / I) / 1000, and an ADC ratio (lesion-ipsilateral thalamus) was calculated in the same manner.[17] Measurements were performed by a single observer.

An independent technique validation analysis was performed to determine the reproducibility of ADC measurements for normal orbital structures. Lacrimal gland ADC was measured by using single small regions of interest on $b = 1000$ and $b = 0$ images, and thalamic ADC was measured in the same manner. Seventeen consecutive patients were analyzed (12 patients at 1.5T, 5 patients at 3T). Images of 2 patients had susceptibility artifact that obscured the lacrimal gland (1 at 1.5T, 1 at 3T).

Statistical Analysis

Values for DWI ratio, ADC, and ADC ratio were compared among orbital lymphoid lesions, OIS, and orbital cellulitis by using the Kruskal-Wallis test. Once a significant difference was determined among the 3 groups, post hoc pairwise comparisons were made by using the Mann-Whitney *U* test. Agreement between the 4 separate lesion ADC measurements was assessed by using the Pearson matrix correlation across all groups ($r = 0.88$, $P < .001$). Additionally, intraobserver agreement between DWI ratio values was assessed by Pearson correlation analysis of a repeat data collection across groups obtained 3 months following the initial collection ($r = 0.98$, $P < .0001$). DWI ratio was compared with ADC ratio by using linear regression analysis ($r = -0.72$, $P = .0036$).

Table 1: T1- and T2-weighted appearance of lesions

Pt. No.	Diagnosis	Appearance	T1 (intensity compared with muscle)	T1 Fat-Saturated Postcontrast (intensity compared with muscle)	T2 (intensity compared with muscle)
1	OIS	Intraconal mass, involving muscle	Isointense	Enhancement > muscle	Isointense
2	OIS	Infiltrative, intra- and extraconal, + lacrimal gland involvement	Isointense	Enhancement > muscle	Hypointense
3	OIS	Infiltrative, thickening of eyelid, + lacrimal gland involvement	Slightly hyperintense	Enhancement > muscle	Hyperintense
4	OIS	Infiltrative, along optic nerve	Motion artifact	Enhancement > muscle	Isointense
5	Lymphoma	Mass just superior to superior rectus muscle	Hyperintense	Enhancement > muscle	Hyperintense
6	Lymphoma	Mass along conjunctiva, preseptal	Hyperintense	Enhancement < muscle	Hyperintense
7	Reactive lymphoid hyperplasia	Inflammatory thickening, retro-orbital fat and eyelid involvement	Isointense	Enhancement = muscle	Hypointense
8	Lymphoma	Inflammatory mass, extraconal	Isointense	Enhancement ≥ muscle	Hyperintense
9	Cellulitis	Infiltrative, pre- and postseptal, + abscess	Isointense	Enhancement > muscle	Hyperintense
10	Cellulitis	Infiltrative, intra- and extraconal	Isointense	Enhancement < muscle	Hyperintense
11	Cellulitis	Infiltrative, intraconal, involving muscle, + abscess	Isointense	Enhancement = muscle	Isointense
12	Cellulitis	Infiltrative, intra- and extraconal	Hyperintense	Enhancement < muscle	Hyperintense
13	Cellulitis	Infiltrative, intra- and extraconal, + abscess	Isointense	Enhancement > muscle	Hyperintense
14	Cellulitis	Infiltrative at orbital apex, + abscess	Isointense	Enhancement > muscle	Hyperintense

Note:—Pt. indicates patient; OIS, orbital inflammatory syndrome.

Results

The T1, T1 postcontrast, and T2-weighted images were evaluated in all patients. All lesions were judged on intensity in comparison with extraocular muscle intensity (Table 1). OIS and lymphoid lesions ranged from to hypo- to hyperintense on T2, whereas orbital cellulitis was typically hyperintense on T2. Most lesions were isointense on T1, and variable degrees of enhancement were seen in all lesions.

On the basis of DWI lesion-thalamic intensity ratio, absolute ADC, and ADC ratio, significant differences were seen, with orbital lymphoid lesions showing the greatest diffusion restriction, cellulitis the least, and OIS an intermediate amount (Table 2). Pairwise comparisons of DWI ratio were significant between all groups ($P < .05$). Lower ADC was seen in lymphoid lesions than in OIS ($P = .04$) or cellulitis ($P = .01$). This difference was often apparent on gross visual inspection of conventional DWI images and on ADC maps, as demonstrated in Figs 1 and 2. Comparison of DWI sequences for OIS lesions seen in Figs 1–3 with cellulitis lesions seen in Figs 4 and 5 also illustrates differences between these lesions. Figure 6 shows the distribution of lesion DWI ratio in a graph form. Pairwise comparison of ADC between OIS and cellulitis showed a similar trend but did not reach statistical significance ($P = .17$). Mild lesion heterogeneity was noted subjectively, as seen in Fig 1 and reflected in correlation analysis of the multiple small measurements obtained in each lesion ($r = 0.88$). ADC showed the expected nonlinear inverse relationship with DWI ratio, and ADC ratio showed the expected inverse linear relationship with DWI ratio. The findings were easily reproduced, with strong correlation between the DWI ratio of the initial dataset and repeat data collection 3 months later ($r = 0.98$).

In our validation analysis, quantitative ADC of the lacrimal gland was $1.39 \pm 0.13 \times 10^{-3}$ mm^2/s, with comparable variability with thalamic ADC in the same group ($0.77 \pm 0.11 \times 10^{-3}$ mm^2/s). Lacrimal gland ADC was in between the observed ADC of OIS and cellulitis lesions, and the DWI ratio for the lacrimal gland was 0.40, also in between the observed DWI ratio of OIS and cellulitis lesions.

Discussion

There are no gold standard diagnostic criteria for differentiating OIS from orbital lymphoid lesion or orbital cellulitis. Diagnosis is based on clinical presentation and response to treatment with some input from CT and MR imaging. However, in light of considerable clinical and imaging overlap, we chose to explore DWI as a tool for increasing the utility of MR imaging at minimal throughput cost.

Analysis of lesion characteristics by T1, T2, and T1 postcontrast sequences did not reveal specific differentiating features. Typically, OIS lesions are described as isointense to extraocular muscle on T1-weighted images but can show variability, which is consistent with our findings.[2,3,6] T2 signal intensity in OIS lesions was less predictable, both in this study and in the literature.[2] OIS lesions showed contrast enhancement, consistent with the literature.[2,18]

Orbital lymphoid lesions were previously noted to be isointense to extraocular muscle on T1.[2,5,18] In our patients, the signal intensity varied from iso- to hyperintensity. Previous studies have not described orbital lymphoid lesions in reference to extraocular muscle on T2.[2,5,18] However, those describing signal intensity in

Table 2: Mean and range of DWI ratios, ADC, and ADC ratios, with statistical comparison

	Lymphoid Lesion	OIS	Cellulitis
Lesion-thalamic DWI ratio*†	1.01 (0.74–1.45); O, C	0.56 (0.43–0.75); L, C	0.31 (0.21–0.49); O, L
Lesion-ADC (10^{-3} mm^2/s)*†	0.78 (0.71–0.95); O, C	1.21 (0.91–1.46); L	1.59 (1.15–2.26); L
Lesion-thalamic ADC ratio*†	0.98 (0.76–1.31); C	1.50 (1.22–1.77)	1.95 (1.46–2.89); L

Note:—C indicates versus cellulitis; O, versus OIS; L, versus lymphoid lesion; DWI; diffusion-weighted imaging; ADC, apparent diffusion coefficient.
*Kruskal-Wallis 1-way analysis of variance of OIS, lymphoid lesion, and cellulitis ($P < .05$).
†Mann-Whitney *U* test ($P < .05$).

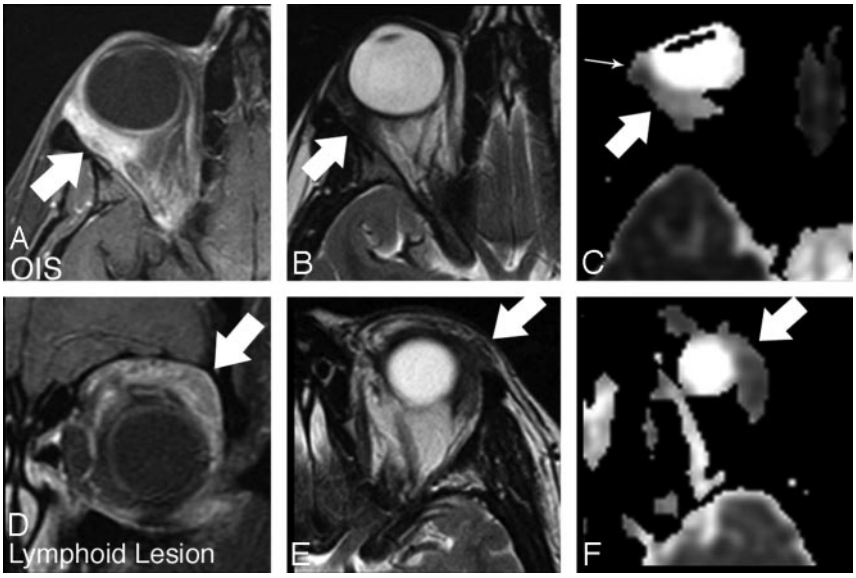

Fig 1. OIS (*A–C*) compared with reactive lymphoid hyperplasia (*D–F*). *A*, Axial T1-weighted fat-suppressed postcontrast image shows intense ill-defined enhancement within the postseptal and retrobulbar fat (*arrow*). *B*, Axial T2-weighted image shows low signal intensity in the area of enhancing abnormality (*arrow*). *C*, Axial ADC image shows moderate signal intensity within the lesion (*arrow*). Slight heterogeneity is noted, with a focal area of slightly lower ADC at the anterior aspect of the lesion (*small arrow*). *D*, Coronal T1-weighted fat-suppressed postcontrast image shows ill-defined enhancement extending throughout the upper extraconal soft tissue (*arrow*). *E*, Axial T2-weighted image shows low signal intensity within the area of enhancing abnormality (*arrow*). *F*, Axial ADC image shows relatively low signal intensity within the lesion compared with the OIS lesion in Fig 1D (*arrow*). Lymphoid lesion ADC intensity is similar to that of brain parenchyma, whereas the OIS lesion shows relatively increased ADC.

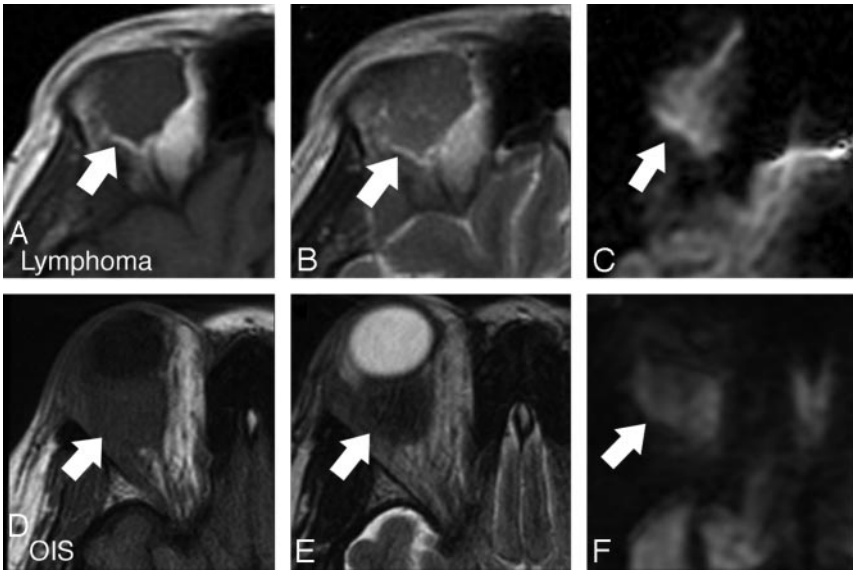

Fig 2. Orbital lymphoma (*A–C*) compared with OIS (*D–F*). *A*, Axial T1-weighted image shows a rounded isointense mass at the upper aspect of the orbit (*arrow*). *B*, Axial T2-weighted image shows isointense signal intensity–to-brain parenchyma (*arrow*). *C*, Axial DWI shows high signal intensity relative to brain parenchyma (*arrow*). *D*, Axial T1-weighted image shows an isointense ovoid intraconal mass (arrow). *E*, Axial T2-weighted image shows slight hypointensity compared with parenchyma (*arrow*). *F*, Axial DWI shows even greater hypointensity compared with brain parenchyma (*arrow*). Comparison of quantitative ADC also showed a difference between these lesions.

relation to orbital fat show inconsistent data.[2,5] Our subjects demonstrated mostly hyperintense T2 signal intensity compared with extraocular muscle. We noted contrast enhancement in all lesions, which is consistent with the literature.[2,18]

Studies of MR imaging of orbital cellulitis are sparse.[6,19,20] Lesions have been previously described as isointense to extraocular muscle and hypointense to orbital fat on T1, with enhancement postcontrast.[6,19,20] We typically noted isointensity to extraocular muscle and variable contrast enhancement. Hyperintensity to extraocular muscle on T2 has been previously described and was consistent with our results.[19]

It is clearly difficult to discern OIS, orbital lymphoid lesions, and orbital cellulitis entirely on the basis of MR imaging. As per the results of this study, DWI can help differentiate these 3 disease processes. We found greater diffusion restriction in lymphoid lesions than in OIS or cellulitis, as measured by DWI intensity and ADC. OIS was significantly brighter on DWI than cellulitis, with a similar trend that did not reach significance on analysis of quantitative ADC. The weakened effect with pairwise comparison of OIS and cellulitis ADC may be attributable to several factors, alone or in combination. T2 shinethrough is a commonly cited phenomenon when apparent diffusion restriction on the DWI sequence is not fully re-

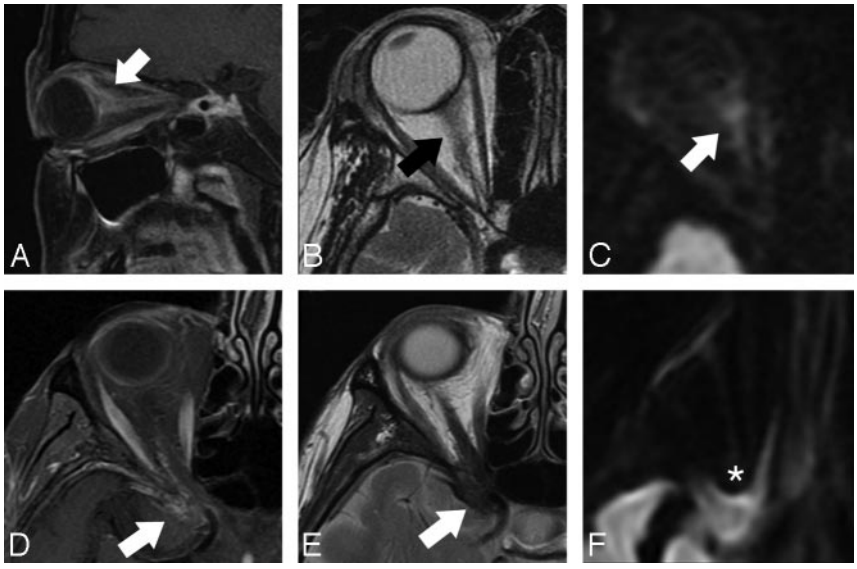

Fig 3. OIS in 2 patients (*A–C, D–F*), showing the relationship between lesion location and susceptibility artifact. *A,* Parasagittal oblique T1-weighted fat-suppressed postcontrast image shows ill-defined enhancement extending along the posterior globe and optic nerve (*arrow*). *B,* Axial T2-weighted image shows isointense signal intensity in the area of enhancing abnormality (*arrow*). *C,* Axial DWI shows moderate signal intensity in this area (*arrow*). *D,* Axial T1-weighted fat-suppressed postcontrast image shows linear irregular enhancement in the region of the orbital apex, extending along the optic nerve course and middle cranial fossa dural surface (*arrow*). *E,* Axial T2-weighted image shows hypointense signal intensity in this area (*arrow*). *F,* Axial DWI demonstrates susceptibility artifact that obscures the lesion (*asterisk*).

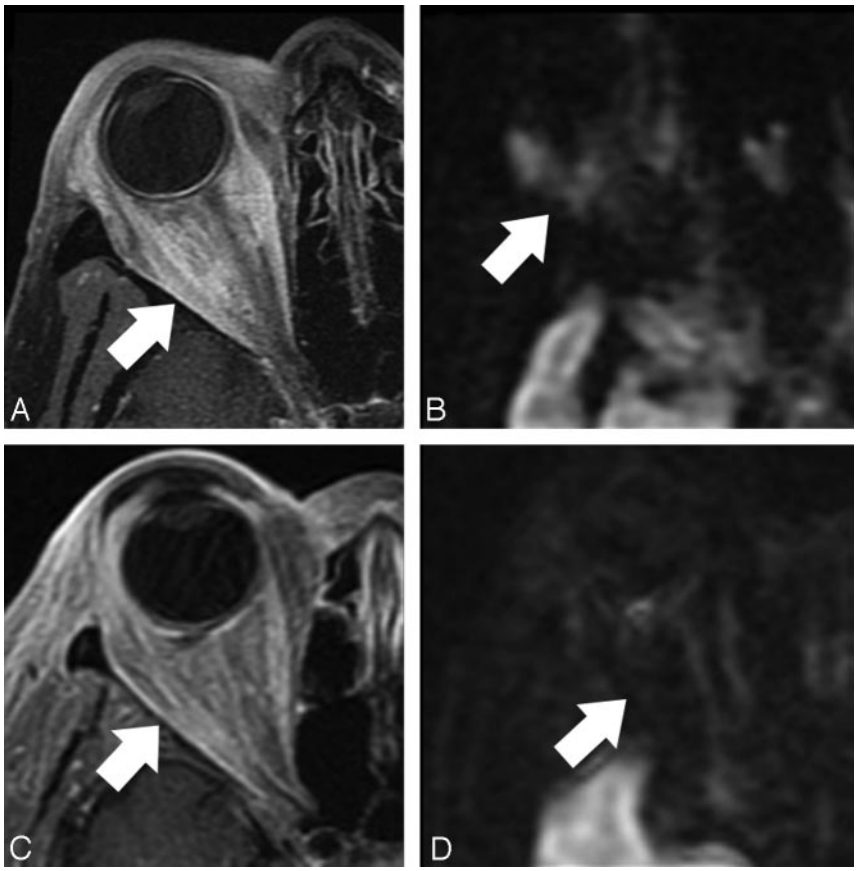

Fig 4. Comparison of a sarcoid lesion (*A* and *B*) with cellulitis (*C* and *D*). *A,* Axial T1-weighted fat-suppressed postcontrast image shows ill-defined enhancement throughout the retrobulbar and periorbital soft tissues (*arrow*). *B,* Axial DWI image shows moderate signal intensity throughout the area of enhancing abnormality (*arrow*). *C,* Axial T1-weighted fat-suppressed postcontrast image shows similar ill-defined retrobulbar and periorbital enhancement (*arrow*). *D,* Axial DWI shows uniform low signal intensity throughout the area of abnormal enhancement (*arrow*).

produced on ADC analysis. A post hoc analysis of lesion-thalamic intensity on $b = 0$ sequences did indeed show that OIS lesions were slightly more hyperintense than cellulitis and also showed that lymphoid lesions were slightly hyperintense compared with OIS lesions. These differences were minimal and did not approach significance ($P = .70$).

Microabscess formation may also decrease ADC in cellulitis lesions, because abscesses are known to restrict diffusion.[21] Finally, inherent measurement error between different techniques may be a contributing factor, particularly with a small sample size. We found moderately strong correlation between DWI ratio and ADC ratio ($r^2 = 0.52$), and the variability between these values may be attributable to any combination of these factors. Despite the overlap in ADC between these lesions, a subset of cellulitis lesions showed a markedly increased ADC, supporting a theory of facilitated diffusion within these lesions.

Differences in cellularity, necrosis, and perfusion may account for differences in diffusion restriction in OIS, orbital lymphoid lesions, and orbital cellulitis. Our findings of restricted diffusion in orbital lymphoid lesion are consistent with expectations. Lymphoid lesions elsewhere in the head and neck region have been noted to restrict diffusion, proba-

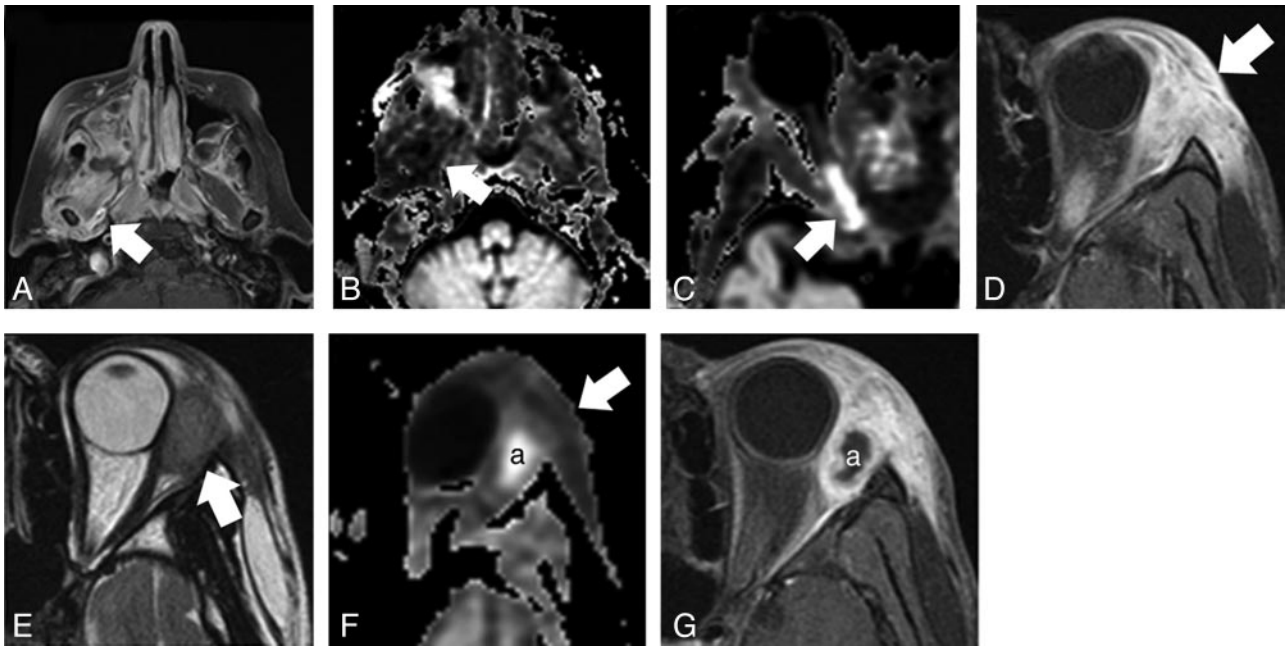

Fig 5. Orbital cellulitis related to mucormycosis (*A–C*) and bacterial infection (*D–F*). *A,* Axial T1-weighted fat-suppressed postcontrast image shows an opacified right maxillary sinus and extensive enhancement throughout the infratemporal fossa tissues, involving the pterygoid muscles (*arrow*). *B,* Axial exponential ADC image shows low intensity throughout these tissues (*arrow*), indicating relatively increased ADC, best appreciated by comparison with the contralateral side. The area of restricted diffusion behind the right maxillary sinus represents abscess. *C,* Axial exponential ADC image through the orbit shows restricted diffusion within the infarcted posterior right optic nerve (*arrow*). *D,* Axial T1-weighted fat-suppressed postcontrast image shows intense enhancement within the periorbital soft tissue (a*rrow*). *E,* Axial T2-weighted image shows moderate hyperintensity relative to extraocular muscle. *F,* Axial exponential ADC image slightly lower shows increased ADC throughout the region of nonspecific enhancement (*arrow*). Restricted diffusion is seen within an abscess (a), which corresponds with a nonenhancing T1 hypointense area. Diffusion is not restricted within the tissues immediately surrounding the focal abscess. *G,* Axial T1-weighted fat-suppressed postcontrast image shows no enhancement within an abscess (a), with marked enhancement in the area of cellulitis.

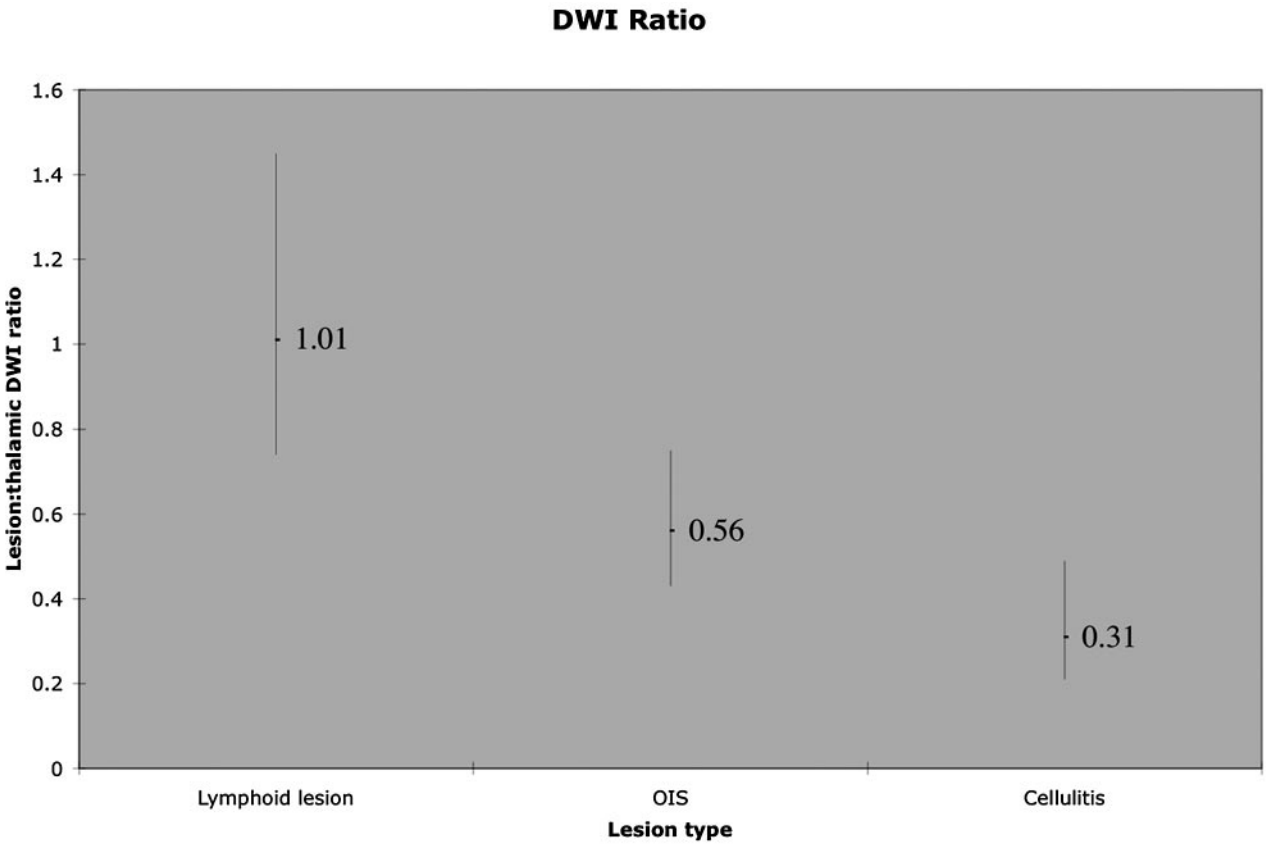

Fig 6. Graph shows lesion-thalamic DWI intensity ratio in patients with orbital lymphoid lesions, OIS, and orbital cellulitis. The mean for each group is given, and a vertical bar depicts the range for each lesion. Orbital lymphoid lesions demonstrate the brightest signal intensities, and OIS lesions are brighter than orbital cellulitis.

bly related to greater cellularity, less extracellular space, and, therefore, less random motion of water.[22] Our findings of increased diffusion in orbital cellulitis relative to both OIS and lymphoid lesions are likely applicable to a larger range of lesions that may be mistaken for cellulitis clinically. Figure 4 shows an example of orbital sarcoid compared with orbital cellulitis, with differences apparent only on DWI. Clinically, this sarcoid lesion was initially mistaken for cellulitis. Even in clinically unequivocal cases, DWI can be valuable for demonstrating complications of cellulitis (Fig 5).

The sample size available in this analysis does not permit parametric analysis and allows only a qualitative statement that the 3 studied entities are distinct from each other with respect to DWI intensity. With a larger sample size, we anticipate being able to perform a quantitative analysis to determine specific values for DWI intensity and ADC that would suggest a particular diagnosis in equivocal cases.

There are specific challenges with DWI of the orbit. DWI is most commonly performed by using echo-planar pulse sequences, which allow rapid imaging times of less than 1 minute. However, application of strong gradients produces magnetic susceptibility artifact, which is most pronounced at interfaces between air, bone, and soft tissue.[23] This is of added concern in the orbit, particularly near the orbital apex, where interfaces with the sphenoid bone and sphenoid sinus notoriously cause susceptibility artifact. Although we often noted some anatomic distortion in the orbit due to these effects, we found that our images were adequate for evaluation if the lesions were $\geq$1 cm in diameter. Two patients were imaged at 3T rather than 1.5T. Increased field strength demands stronger gradient pulses, with an associated increase in magnetic susceptibility artifact. We noticed more anatomic distortion at 3T but were able to obtain consistently high-quality DWI, and no subjects in the current investigation were excluded on the basis of artifact attributable primarily to higher field strength. The use of ASSET parallel acquisition was likely an important factor in achieving consistently adequate images of the orbit.

In our validation analysis, we were able to visualize the lacrimal gland with DWI in 15/17 patients and were able to obtain consistent ADC and DWI ratio values for this structure, supporting the claim that the orbit can be reliably assessed with whole-brain echo-planar DWI sequences. However, we recognize that performance depends on many variables and would suggest that a similar validation study be performed before applying these techniques to patients in other institutions. Manual ADC calculation may have limited our precision, and automated ADC calculation would likely be more precise and easily performed. Future investigations of DWI in the orbit may also benefit from the use of alternative techniques that help minimize susceptibility artifact. Different parallel acquisition techniques such as generalized autocalibrating partially parallel acquisition may show better performance in the orbit, and turbo spin-echo DWI has been described as advantageous in imaging middle ear cholesteatoma.[24] Continued efforts to improve DWI techniques in the head and neck will likely allow expanded uses of this valuable tool.

Conclusions

It is apparent that conventional CT and MR imaging for OIS, orbital lymphoid lesions, and orbital cellulitis, though useful, may not always lead to a conclusive diagnosis. This limited series provides promising preliminary data on the utility of DWI in clinically undifferentiated cases of OIS, orbital lymphoid lesions, and orbital cellulitis, showing that these entities are distinct from each other with respect to features on DWI. A larger study would better determine the specificity and sensitivity of DWI imaging in differentiating OIS from other orbital conditions and would potentially allow quantitative discrimination between different lesions. Although we were able to obtain satisfactory images in nearly all cases by using a whole-brain echo-planar DWI sequence with parallel acquisition, future exploration into targeted orbit DWI and alternative DWI techniques that are less sensitive to magnetic susceptibility artifact may be valuable.

References

1. Karesh JW, Baer JC, Hemady RK. **Noninfectious orbital inflammatory disease.** In: Tasman W, Jaeger EA, eds. *Duane's Clinical Ophthalmology.* Philadelphia: Lippincott Williams & Wilkins, 2005:1–45
2. Uehara F, Ohba N. **Diagnostic imaging in patients with orbital cellulitis and inflammatory pseudotumor.** *Int Ophthalmol Clin* 2002;42:133–42
3. Atlas SW, Grossman RI, Savino PJ, et al. **Surface-coil MR of orbital pseudotumor.** *AJR Am J Roentgenol* 1987;148:803–08
4. Weber AL, Vitale Romo L, Sabates NR. **Pseudotumor of the orbit: clinical, pathologic, and radiologic evaluation.** *Radiol Clin North Am* 1999;37:151–68
5. Valvassori GE, Sabnis SS, Mafee RF, et al. **Imaging of orbital lymphoproliferative disorders.** *Radiol Clin North Am* 1999;37:135–50
6. Cytrn AS, Putterman AM, Schneck GL, et al. **Predictability of magnetic resonance imaging in differentiation of orbital lymphoma from orbital inflammatory syndrome.** *Ophthal Plast Reconstr Surg* 1997;13:129–34
7. Le Bihan D, Breton E, Lallemand D, et al. **MR imaging of intravoxel incoherent motions: application to diffusion and perfusion in neurologic disorders.** *Radiology* 1986;161:401–07
8. Kono K, Inoue Y, Nakayama K, et al. **The role of diffusion-weighted imaging in patients with brain tumors.** *AJNR Am J Neuroradiol* 2001;22:1081–88
9. Stadnik TW, Chaskis C, Michotte A, et al. **Diffusion-weighted MR imaging of intracerebral masses: comparison with conventional MR imaging and histologic findings.** *AJNR Am J Neuroradiol* 2001;22:969–76
10. Castillo M, Smith JK, Kwock L, et al. **Apparent diffusion coefficients in the evaluation of high-grade cerebral gliomas.** *AJNR Am J Neuroradiol* 2001;22:60–64
11. Tien RD, Felsberg GJ, Friedman H, et al. **MR imaging of high-grade cerebral gliomas: value of diffusion-weighted echo planar pulse sequences.** *AJR Am J Roentgenol* 1994;162:671–77
12. Johnson BA, Fram EK, Johnson PC, et al. **The variable MR appearance of primary lymphoma of the central nervous system: comparison with histopathologic features.** *AJNR Am J Neuroradiol* 1997;18:563–72
13. Wang J, Takashima S, Takayama T, et al. **Head and neck lesions: characterization with diffusion-weighted echo-planar MR imaging.** *Radiology* 2001;220:621–30
14. Rusakov DA, Kullman DM. **Geometric and viscous components of the tortuosity of the extracellular space in the brain.** *Proc Natl Acad Sci U S A* 1998;95:8975–80
15. Westacott S, Garner A, Moseley IF, et al. **Orbital lymphoma versus reactive lymphoid hyperplasia: an analysis of the use of computed tomography in differential diagnosis.** *Br J Ophthalmol* 1991;75:722–25
16. Rumboldt Z, Camacho DLA, Lake D, et al. **Apparent diffusion coefficients for differentiation of cerebellar tumors in children.** *AJNR Am J Neuroradiol* 2006;27:1362–69
17. Zhou XJ, Leeds NE, McKinnon GC, et al. **Characterization of benign and metastatic vertebral compression fractures with quantitative diffusion MR imaging.** *AJNR Am J Neuroradiol* 2002;23:165–70
18. Yan J, Wu Z, Li Y. **The differentiation of idiopathic inflammatory pseudotumor from lymphoid tumors of orbit: analysis of 319 cases.** *Orbit* 2004;23:245–54
19. Eustis HS, Mafee MF, Walton C, et al. **MR imaging and CT of orbital infections and complications in acute rhinosinusitis.** *Radiol Clin North Am* 1998;36:1165–83
20. Atlas SW, Bilaniuk LT, Zimmerman RA, et al. **Orbit: initial experience with surface coil spin-echo MR imaging at 1.5T.** *Radiology* 1987;164:501–09
21. Schaefer PW, Grant PE, Gonzalez RG. **Diffusion-weighted MR imaging of the brain.** *Radiology* 2000;217:331–45
22. Kind AD, Ahuja AT, Yeung DK, et al. **Malignant cervical lymphadenopathy: diagnostic accuracy of diffusion-weighted MR imaging.** *Radiology* 2007;245:806–13
23. Mafee MF, Rapoport M, Karimi A, et al. **Orbital and ocular imaging using 3- and 1.5-T MR imaging systems.** *Neuromaging Clin N Am* 2005;15:1–21
24. De Foer B, Vercruysse J, Pilet B, et al. **Single-shot, turbo spin-echo, diffusion-weighted imaging versus spin-echo-planar, diffusion-weighted imaging in the detection of acquired middle ear cholesteatoma.** *AJNR Am J Neuroradiol* 2006;27:1480–82